

Jane P. Ko, MD
 Henry Rusinek, PhD
 Erika L. Jacobs, MD
 James S. Babb, PhD
 Margrit Betke, PhD
 Georgeann McGuinness, MD
 David P. Naidich, MD

Index terms:

Computed tomography (CT), image processing, 60.12117
 Computed tomography (CT), technology, 60.12117
 Images, analysis, 60.12117
 Lung, CT, 60.12117
 Lung, nodule, 60.12117

Published online

10.1148/radiol.2283020059
Radiology 2003; 228:864–870

Abbreviations:

FTM = fixed-threshold method
 PVM = partial-volume method
 ROI = region of interest
 VTM = variable-threshold method

¹ From the Department of Radiology, Section of Thoracic Imaging, New York University Medical Center, 560 1st Ave, New York, NY 10016 (J.P.K., H.R., E.L.J., G.M., D.P.N.); Fox Chase Cancer Center, Philadelphia, Pa (J.S.B.); and Computer Science Department, Boston University, Mass (M.B.). From the 2001 RSNA scientific assembly. Received February 7, 2002; revision requested April 15; final revision received October 28; accepted December 19. Supported by a Scholars Award from the RSNA Research and Education Foundation and a Seed Grant from the Society of Thoracic Radiology. **Address correspondence** to J.P.K. (e-mail: jane.ko@med.nyu.edu).

Author contributions:

Guarantors of integrity of entire study, J.P.K., H.R.; study concepts and design, J.P.K., H.R.; literature research, J.P.K.; experimental studies, J.P.K., E.L.J., H.R.; data acquisition and analysis/interpretation, J.P.K., E.L.J., H.R.; statistical analysis, J.S.B.; manuscript preparation, J.P.K., H.R.; manuscript definition of intellectual content, J.P.K., H.R., D.P.N.; manuscript editing, revision/review, and final version approval, all authors.

© RSNA, 2003

Small Pulmonary Nodules: Volume Measurement at Chest CT—Phantom Study¹

Three-dimensional methods for quantifying pulmonary nodule volume at computed tomography (CT) and the effect of imaging variables were studied by using a realistic phantom. Two fixed-threshold methods, a partial-volume method (PVM) and a variable method, were used to calculate volumes of 40 plastic nodules (largest dimension, <5 mm: 20 nodules with solid attenuation and 20 with ground-glass attenuation) of known volume. Tube current times (20 and 120 mAs), reconstruction algorithms (high and low frequency), and nodule characteristics were studied. Higher precision was associated with use of a PVM with predetermined pure nodule attenuation, high-frequency algorithm, and diagnostic CT technique (120 mAs). A PVM is promising for volume quantification and follow-up of nodules.

© RSNA, 2003

Chest computed tomography (CT) is a sensitive method for detecting pulmonary nodules. Detection of small pulmonary nodules is improved by imaging the lung parenchyma in thin transverse CT sections. Nodules larger than 1 cm in largest dimension have a higher likelihood of malignancy (1), and they are amenable to further evaluation with transthoracic needle aspiration biopsy (2), contrast material-enhanced CT (3), and fluorine 18 fluorodeoxyglucose positron emission tomography (4). While nodules smaller than 1 cm are more difficult to characterize and more commonly benign than are larger nodules, they do not preclude malignancy (5,6). Unfortunately, morphologic CT characteristics, such as the presence of calcification and nodule margins, are unreliable for differentiation of benign from malignant nodules (7,8) and may be difficult to assess

when nodules are 5 mm or smaller in largest dimension.

As a consequence, attention has been focused on nodule growth to differentiate malignant from benign nodules. Malignant nodules typically double in volume between 30 days and 14 months (9,10). Doubling times of less than 30 days are usually associated with inflammatory or infectious causes. Although times longer than 14 months have been associated with benign nodules such as hamartomas (9), it should be emphasized that some bronchioloalveolar carcinomas, especially those appearing as a ground-glass nodule, have been reported as having doubling times with a mean of 880 days (11).

Currently, nodule measurement is typically assessed in two dimensions rather than in three dimensions. Unfortunately, measurements performed by radiologists are subject to inter- and intraobserver variations (12–14). Therefore, attention has focused on two-dimensional area and three-dimensional computer-aided quantitative volume measurement algorithms that depend on nodule segmentation by means of gray-level thresholds. Such three-dimensional approaches are promising in that they minimize variation and decrease measurement error (15,16).

Volume quantification of ground-glass nodules and non-threshold-based quantitative methods that minimize partial-volume effects have not been studied extensively (17). Volumes of ground-glass nodules are more difficult to measure secondary to their lower contrast to the lung parenchyma compared with those of solid soft-tissue attenuation nodules. The low-dose CT technique, introduced to limit radiation exposure to patients (5,18,19) and commonly used to screen high-risk individuals for lung cancer, has not been investigated extensively in terms of its effect on nodule quantification. Choices of reconstruction algorithm, nodule size, and thoracic geometry have been shown to affect measurement of nodule attenuation (20,21)

and potentially may affect quantification of nodule volume.

Thus, the purpose of our study was to compare a variety of three-dimensional methods for quantifying pulmonary nodule volume at chest CT and to study the effect of imaging variables.

I Materials and Methods

Phantom

A chest CT phantom (Computerized Image Reference Systems, Norfolk, Va) was used to replicate a 5-cm-thick transverse section of a human thorax and was composed of materials simulating muscle, fat, bone, and lung. The phantom was a variation of one that was used for studies on nodule densitometry (1,22). Twenty 8-mm-diameter wells were drilled into the plastic material of each lung. Four wells each were placed in the periphery of each lung along the anterior, medial, posterior, and lateral pleural surfaces, and four wells were placed in the center of the lung. Peripheral wells were placed so that the edge closest to the pleura was 10, 5, 2.5, or 0 mm away from the pleural surface.

Forty manufactured approximately spherical nodules were studied. The nodules were composed of a plastic created by blending epoxy resins and urethanes. Twenty simulated ground-glass nodules had attenuations of approximately -360 HU, and 20 simulated solid nodules had attenuations of approximately 50 HU. There were four nodule size categories for each nodule attenuation. Each size category had five nodules. The four nodule sizes were selected so that their approximate diameters were larger than 2 mm and smaller than 5 mm. To obtain their true volumes, the nodules were weighed two times on a precision scale (model AJ100; Mettler Toledo, Columbus, Ohio) that was capable of 1 -mg accuracy. For the few cases with a discrepancy greater than 0.5 mg between the two weights, the nodule was weighed a third time, and all three measurements were averaged. The true volume of a nodule was calculated by multiplying the nodule weight by the specific gravity of the material used to construct the nodule. Two values of specific gravity, one for ground-glass nodules and the other for solid-attenuation nodules, were provided by the manufacturer and verified in our laboratory. Specific gravity of each material was verified by means of precision machining of a cylinder with diameter (d) of 40 mm and height (h) of 20 mm. The exact largest dimensions were measured with pre-

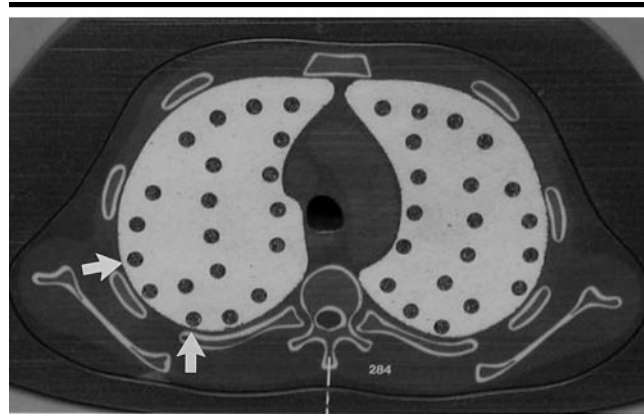


Figure 1. Photograph of chest phantom demonstrates wells (arrows, $n = 40$) filled with material with the same attenuation as that of lung parenchyma. Material obscures nodules placed in the wells.

cision calipers (± 0.1 mm) and used to calculate volume [$\pi h(d/2)^2$]. Each cylinder was weighed three times on the precision scale, and the specific gravity was calculated by dividing weight by volume. We estimated the nodule volumes to be accurate within 0.5% .

One nodule was placed into each well and surrounded by a mixture created so that its mean attenuation (-786 HU) was equivalent to that of the phantom lung parenchyma (-780 HU) (Fig 1). The loose mixture presented a realistic background with fine texture. The mixture was composed of two relatively homogeneous particulate materials, one with lower attenuation (ground marjoram, 72%) and the other with higher attenuation (ground coffee, 28%) compared with that of the phantom lung parenchyma. The materials were selected from a number of particulate materials that had been imaged with CT and measured for attenuation. The relative proportions of coffee and marjoram were determined by solving a linear equation with the desired attenuation of the final mixture and the known attenuations of the two materials. CT images showed no air pockets at the interface of the nodule and the surrounding mixture. Each phantom region (eg, anterior, posterior) had one nodule of each size category, and the ground-glass and solid-attenuation nodules were placed in the left and right lungs, respectively. We assumed no difference in measurement error between right and left lung location.

CT Imaging

The phantom was imaged with a multi-detector row CT scanner (Somatom Volume Zoom Plus 4; Siemens Medical Solutions, Iselin, NJ) with the standard

protocol for chest CT at New York University. Imaging was performed with a 140 -kV potential and 0.5 -second rotation speed. Data were reconstructed in 1.25 -mm-thick transverse sections at 1.0 -mm intervals with a 30 -cm field of view. The phantom was imaged by using all permutations of 20 and 120 mAs, which are typically used to perform low-dose (23) and diagnostic CT, respectively, and low- and high-frequency reconstruction algorithms (Fig 2).

Nodule Volume Quantification

Volume analysis was performed with a standard commercially available workstation (Wizard; Siemens Medical Solutions). Images were analyzed without knowledge of the true volume of a nodule or the calculated volume based on measurements. The images were displayed with standard window width of $1,600$ HU and center of -600 HU, and the images that demonstrated a nodule were analyzed. Additionally, one image above and one image below the visualized nodule were analyzed to ensure measurement of the entire nodule, in case volume averaging led to poor visualization of the nodule in its most cranial or caudal transverse section. Volumes of the nodules in the transverse sections that were analyzed were summed to obtain the total volume of the nodule.

Nodule volume was analyzed with variations of a partial-volume method (PVM) and a binary threshold method. Two types of threshold methods, a variable-threshold method (VTM) and a fixed-threshold method (FTM), were used. The PVM was based on the fact that the mean attenuation in a region of interest (ROI) drawn around a nodule ("large ROI") was reflective of the proportions and attenuation of

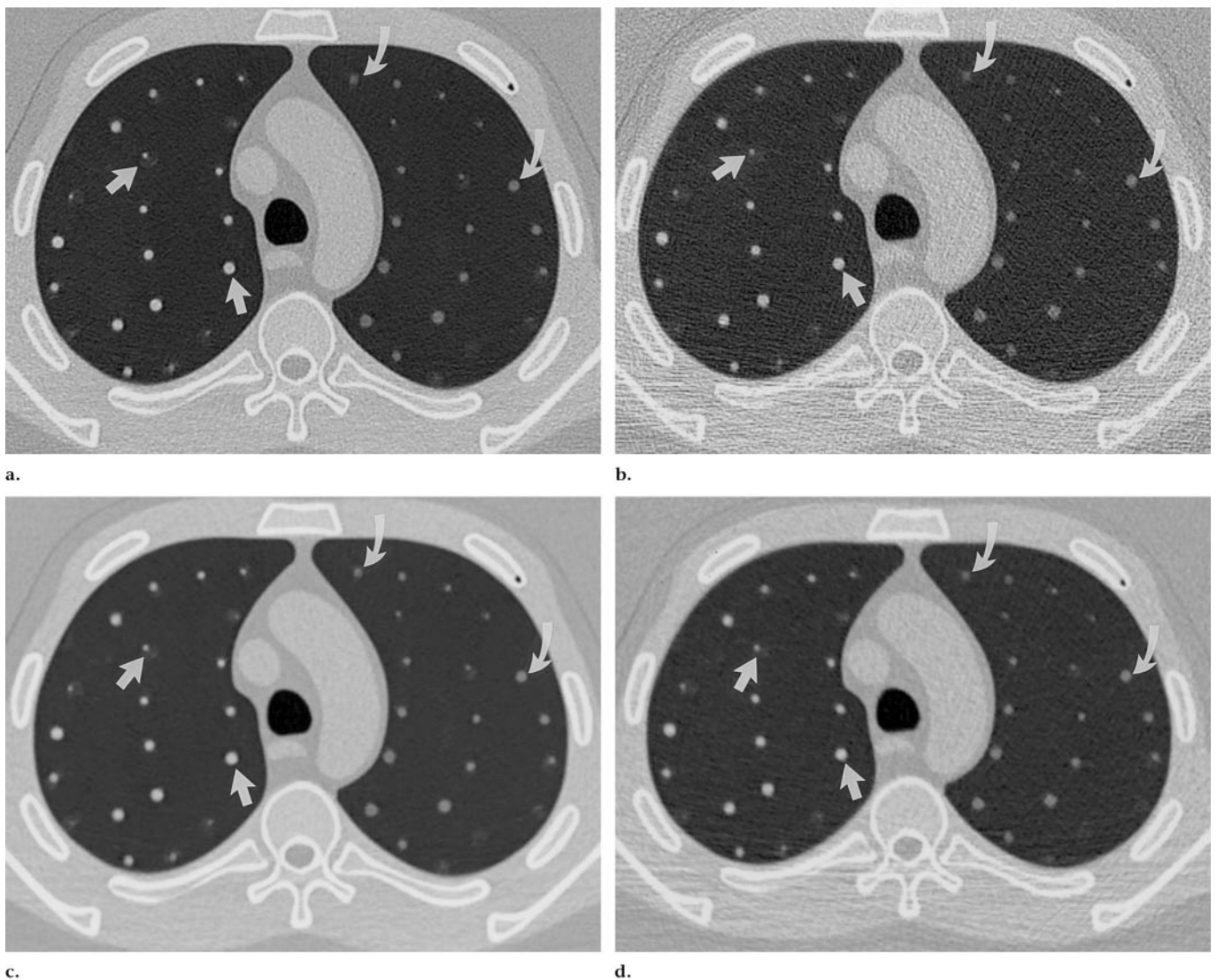


Figure 2. Transverse CT scans of the nodule-containing phantom. Ground-glass-attenuation nodules (curved arrows) and solid-attenuation nodules (straight arrows) are in the left and right lungs of the phantom, respectively, surrounded by heterogeneous material. Images were obtained with variations of dose and reconstruction algorithm: (a) 120-mAs dose and high-frequency reconstruction algorithm, (b) 20-mAs dose and high-frequency reconstruction algorithm, (c) 120-mAs dose and low-frequency reconstruction algorithm, and (d) 20-mAs dose and low-frequency reconstruction algorithm. The 20-mAs low-dose images (b, d) have more image noise. On the low-frequency-algorithm images (c, d), spatial resolution is decreased.

structures contained within. The large ROI included about 3 mm of lung tissue along the circumference of a nodule. The relationship $V_r \times A_r = V_n \times A_n + (V_r - V_n) \times A_l$ was used to solve for V_n , the volume of the nodule in a transverse section. V_r was the volume of the large ROI, A_r was the mean attenuation in the large ROI, A_n was the pure nodule attenuation, and A_l was the pure lung attenuation. When measured, A_n was obtained from the image on which the nodule was most conspicuous; at least 20 voxels of the central region of a nodule were measured, except for the smallest nodules (approximately 2.5 mm), in which at least 5 voxels in the center

were sampled. A_l was obtained by averaging three lung attenuation measurements adjacent to the nodule for each transverse section analyzed.

For the threshold methods, the voxels above a threshold value in the large ROI were counted. For the simplest strategy, which was the FTM, a threshold of -500 HU was applied to all images analyzed for each nodule. For the VTM, the attenuation threshold value was an average between A_n obtained for the PVM and the mean of five pure lung attenuation measurements obtained from the general lung. The nodule volume per transverse section was calculated by multiplying the

number of voxels above the threshold by the voxel volume.

Since the value of the pure nodule attenuation was suspected to contribute critically to the variance in the volume estimates, variations of the PVM and threshold methods (VTM and FTM) were studied. These variants differed in terms of the definition of the pure nodule attenuation (Table 1). PVM1 and VT1 may be clinically applicable only when multiple nodules are present. With PVM2 and VTM2, pure nodule attenuation is sampled from each nodule being measured, regardless of its size. In the variant PVMA, assumed pure nodule attenuation

values were used (−380 HU for ground-glass-attenuation nodules and 20 HU for solid-attenuation nodules) that were fixed but were about 20 HU less than the true attenuation values of the nodules.

ROIs were manually placed on the images and recorded attenuation and voxel number results. To summarize the sampling scheme, our phantom had 40 nodules (four nodule size categories, two nodule attenuation categories, and five individual nodules in each of the eight size and attenuation categories) placed at different locations in the phantom. The phantom was imaged twice with two different tube current times, and each acquisition was reconstructed by means of two reconstruction algorithms, which yielded 160 nodule image sets. All of the sets were measured once by one observer (E.L.J.) with each of the six measurement methods, which yielded 960 measurements.

Several weeks later, this observer repeated each of the six measurement methods with 24 randomly selected nodule image sets, which led to 144 measurements, without knowledge of the previous ROI locations and measurement results. Without knowledge of the results obtained by the first observer, a second observer (J.P.K.) performed each of the six measurements on 60 nodule image sets, which comprised 20 ground-glass-attenuation nodules imaged at 120 and 20 mAs ($n = 40$ nodule image sets) and 20 solid-attenuation nodules imaged at 20 mAs ($n = 20$ sets), which yielded 360 measurements. The 60 image sets were selected to include ground-glass-attenuation nodules with 20-mAs technique, given the likelihood that measurements could be affected by lower contrast and higher image noise in these scenarios. One observer (E.L.J.) measured the smallest distance of a nodule to the pleura by using the electronic calipers on the workstation.

Data Analysis

Let $V_{p,r}$ denote the measured volume of a nodule, where the lumped index p represents the unknown characteristics of the nodule (such as size and attenuation) and the lumped index r represents the known measurement characteristics (tube current time, reconstruction algorithm, computational algorithm). Owing to the imaging limitations, such as CT collimation (imperfect section profile) and in-plane spatial resolution, we expect a relationship $V_{p,r} = K_r T_p$ where $K_r \sim 1$ is a multiplicative bias of the method and T_p is the true volume of a nod-

TABLE 1
Volume Measurement Methods

Abbreviation	Pure Nodule Attenuation
PVMA	Assumed to be −380 HU for ground-glass-attenuation nodules and 20 HU for solid-attenuation nodules
PVM1	Obtained from largest nodule in lung region (anterior, medial, central, posterior, lateral), approximately 5 mm
PVM2	Obtained from each nodule measured
VTM1	Obtained from largest nodule in lung region, approximately 5 mm
VTM2	Obtained from each nodule measured
FTM	−500 HU

ule. In the first stage of data analysis, we calibrated the measurements to eliminate the multiplicative bias due to the imaging imperfections. For each value of index r , we used the least-squares fit of the subset of measured values to the true data to derive the factors K_r . These factors will be used in our future clinical measurements of nodule volume and growth. We calibrated the measured volumes and computed the absolute error (AE) of each technique as $AE_{p,r} = |V_{p,r}/K_r - T_p|$. The absolute residual difference between the true and bias-corrected observed volumes, or absolute error, was interpreted as a measure of precision.

The absolute errors were analyzed statistically by means of repeated measures analysis of variance that incorporated correlations introduced through the bias adjustment. Since a single least squares estimate of the slope parameter was used to adjust all volume assessments in a bias group, the absolute errors in a bias group are correlated. Initially, the model included the following as fixed effects: nodule location, nodule size, nodule attenuation, reconstruction algorithm, tube current times, nodule distance from the pleura, and measurement method, as well as all two-factor interactions among these factors. Bias group was included as a random factor. Nodule size and distance from the pleura were treated as numeric rather than ordinal categorical factors. This implies that the effect of each factor on absolute error is linear, and there was no indication in the data to refute this assumption. P values reflected the effect of a given factor after adjustment for the effects of all other factors. Methods were combined into groups and compared in terms of mean absolute error. Inter- and intraexaminer reliability of each method was assessed by means of the fixed effects interclass correlation coefficient (24). The coefficients were calculated with 95% CIs. Differences in bias were tested by means of the Student t test. Statistical analysis was performed (SAS; SAS Institute, Cary, NC).

TABLE 2
Factors with Significant Effect on Absolute Error

Factor	F Value	P Value*
Size	94.96	<.001
Attenuation	5.20	.023
Tube current time	25.05	<.001
Method	4.13	.001
Method by size	32.29	<.001
Method by attenuation	6.88	<.001
Method by tube current time	2.25	.049

* Analysis of variance.

Results

True volumes of the four nodule size categories were $60.7 \text{ mm}^3 \pm 2.0$, $35.0 \text{ mm}^3 \pm 1.4$, $18.0 \text{ mm}^3 \pm 0.8$, and $7.5 \text{ mm}^3 \pm 1.2$. Corresponding diameters, assuming the nodules were spheres, were on average 4.9, 4.0, 3.2, and 2.4 mm, respectively. Distances of the nodules from the pleura ranged between 1 and 38 mm.

By using the 960 observations (960 = six methods \times two tube current times \times two reconstruction algorithms \times two nodule densities \times five locations \times four sizes), the tube current time, reconstruction algorithm, quantitative method, nodule attenuation, and nodule size significantly ($P < .001$) affected the volume error. No significant effect on volume error was noted for nodule location ($P = .18$) or distance from the pleura ($P = .83$).

Nodule volume measured on images reconstructed with a high-frequency reconstruction algorithm (mean absolute error = 3.0 mm^3) was more precise than that measured on images reconstructed with a low-frequency algorithm (mean absolute error = 3.7 mm^3) ($P = .002$). A high-frequency reconstruction algorithm significantly interacted with both method ($P < .001$) and attenuation ($P < .001$). This implies that in terms of minimizing the expected mean absolute er-

TABLE 3
Error in Nodule Volume Measurements: Effect of Tube Current Time

Approximate Nodule Volume (mm ³)	Mean Absolute Error (mm ³)	
	120 mAs*	20 mAs
8	1.5	2.0
18	2.4	3.0
35	2.9	4.0
61	3.8	4.7

* Smaller error than that for 20 mAs averaged over different nodule volumes (analysis of variance, $P < .001$).

TABLE 4
Error in Nodule Volume Measurements: Effect of Method and Nodule Attenuation

Method	Nodule Attenuation		
	Ground Glass	Solid	Combined
PVM			
PVMA	1.6	1.7	1.6
PVM1	2.0	1.9	1.9
PVM2	2.2	2.4	2.3
Threshold			
VTM1	2.2	2.4	2.3
VTM2	2.8	2.5	2.7
FTM	8.4	5.7	7.0

Note.—Data are mean absolute errors (mm³). Significant interaction between method and attenuation (analysis of variance, $P < .001$).

ror, the choice of optimal algorithm might depend on the method of measurement and/or nodule attenuation. However, a high-frequency algorithm had a lower mean absolute error with all methods of measurement, irrespective of nodule attenuation. Hence, the high-frequency algorithm was determined to be superior to the low-frequency algorithm under the conditions investigated in this study. Consequently, the analyses were redone, and all subsequent results pertain only to the data obtained with the high-frequency algorithm. Factors with significant effects on mean absolute error with this analysis are listed in Table 2.

Mean absolute error for nodules imaged at 120 mAs was significantly smaller than that for nodules imaged at 20 mAs for all nodule sizes and measurement methods (Table 3). After adjustment for differences due to other factors that were varied in the study, change from a high-dose to a low-dose technique added at least 0.48 mm³ and a mean 0.86 mm³ to

the absolute error. Absolute errors for ground-glass-attenuation nodules were higher than those for solid-attenuation nodules ($P = .02$) (Table 4).

Results obtained with the PVM were more precise than those with the FTM for both solid- and ground-glass-attenuation nodules ($P < .001$) (Table 4). The methods had significant interaction with size, dose, and attenuation. The PVMs as a group (PVMA, PVM1, PVM2) had a significantly lower mean absolute error than did the threshold methods (FTM, VTM1, VTM2) ($P = .0278$) and the VTMs (VTM1, VTM2) ($P = .0285$) (Table 5). Results with the PVMs had lower mean absolute error than did the threshold methods (FTM, VTM1, VTM2) for small ($P = .0092$) or large ($P = .0377$) nodules (Table 6). Mean absolute error for PVMA was significantly lower ($P = .04$) than that for the other two PVMs (PVM1, PVM2) combined when the errors were averaged over the levels of all other factors.

Interclass correlation coefficients for interexaminer reliability were 0.98 (95% CI: 0.95, 0.99) for VTM1, 0.99 (95% CI: 0.97, 1.00) for PVM1, and 0.99 (95% CI: 0.98, 1.00) for PVMA. Intraexaminer interclass correlation coefficients for these three methods were also excellent, all greater than 0.99 (95% CI: 0.98, 1.00).

Systematic multiplicative measurement bias (true volume divided by calculated volume) of the volume measurements with all variants of the PVMs was 0.91 ± 0.04 . Bias of measurements with the threshold methods was 1.06 ± 0.09 for VTM1, 0.99 ± 0.18 for VTM2, and 0.99 ± 0.07 for FTM. Bias of measurements with the low-dose technique was 0.94 ± 0.07 , and that with the high-dose technique was 0.99 ± 0.08 ($P = .001$), which was closer to the value 1.0.

Discussion

Given the need for close monitoring of patients with lung nodules at chest CT, there is interest in determining the optimal method to identify change in nodule size precisely and consistently. About one-quarter to one-half of patients who undergo screening CT for lung cancer have one to six noncalcified nodules (5,25). More than half the detected nodules were smaller than 5 mm in largest dimension (5). These nodules are generally too small to be evaluated further with any currently available option except follow-up CT.

One-dimensional (26) or two-dimensional (12) perpendicular measurements

are used in oncology practice to measure lesion size and any change in size over time; however, they are suboptimal. The extent of a nodule in the craniocaudal direction at transverse imaging is overlooked. Results of measurements of lesions by human observers are affected by interobserver variability and are reduced when radiologists are assisted by a semi-automated autocontour technique for measuring two-dimensional perpendicular diameters (12). Measurements of nodules are affected by partial-volume averaging, which makes size estimates susceptible to window display settings and section thickness (13).

Three-dimensional methods applied to thin-section CT images enable accurate assessment of nodule size by means of quantification of nodule volume (15,16). Yankelevitz et al (16) reported use of two-dimensional and three-dimensional semi-automated thresholding techniques for volume measurement. For small solid spherical nodules that were imaged in air with 1.0- and 0.5-mm-thick sections with a single-detector row helical CT scanner, volume errors of 2.88% and 1.05%, respectively, were demonstrated for 3–6-mm nodules (16). When the spheres were deformed, an increase in volume error to 3% on 1.0-mm-thick sections and a significant advantage of three-dimensional over two-dimensional methods were demonstrated for volume measurement.

Despite high-resolution imaging with 1-mm-thick sections, three-dimensional measurement of nodule volume for small nodules approximately 3–5 mm in largest dimension is affected by partial-volume averaging (16). Previous methods that addressed quantification of structures and nodule volume were typically based on thresholding algorithms (12,15,16,27). Thresholding algorithms, which apply attenuation criteria to identify voxels as belonging either to a nodule or background, may not detect or may classify as 100% the peripheral voxels of a nodule, which are most susceptible to partial-volume effect.

Results in our phantom experiment demonstrate that the PVMs have higher precision for measuring volumes, possibly because the effect of partial-volume averaging is reduced. The lower mean absolute error with the PVMs was significant, particularly for 20 mAs, which is typically used with low-dose CT. Moreover, results with the variant PVMA had an advantage over those with the other two methods in the group of PVMs. Therefore, we conclude that for precise measurement of small lung nodules, PVMs should use assumed rather than

sampled nodule attenuation for respective solid- and ground-glass-attenuation nodules. Difficulty in measuring nodule attenuation, particularly of small nodules, was demonstrated in previous studies on nodule densitometry (20,21,28). Multiple variables consistently influenced the measurement of nodule attenuation, particularly the reconstruction algorithm (20,21), nodule size (20), and partial-volume effect (20,28). Nodules with mixed ground-glass- and solid-attenuation components have been described with adenocarcinoma (11). Monitoring for the growth of mixed attenuation nodules is feasible, provided that a pure nodule attenuation measurement is maintained for calculating volumes on initial and follow-up studies and provided that the proportions of solid and ground-glass attenuations do not change. However, one should be aware that if PVMs are used, an increase in the solid component of a subsolid nodule may be interpreted falsely as an increase in volume.

When all methods were included, we demonstrated a significantly higher volume error for measurement of ground-glass-attenuation nodules as opposed to that for measurement of solid-attenuation nodules. While more work is needed to assess the error as a function of nodule attenuation, we hypothesize that any differences between methods for ground-glass-attenuation nodules are related to the reduced contrast between the ground-glass nodule and the lung parenchyma. Decreased contrast makes binary threshold segmentation of the nodule from surrounding lung tissue more difficult. The realistic lung background in our phantom and the use of a 30-cm field of view might explain the larger volume errors (1.2–10.0 mm³ for 8–60-mm³ nodules) compared with those in previous studies on solid-attenuation nodules in air (3% error) (16).

The primary clinical use of volume measurements is monitoring of the growth rate of pulmonary nodules. Results in the current study can be used with the probability theory to estimate errors in growth rate. With the precision of 2.1 mm³ that we obtained in our phantom experiment, the SD for assessment of the 20% growth of a 50-mm³ nodule would be 6.5%, which would translate to a 95% CI of 7%, 33%. In the case of the 20% growth of a smaller 12-mm³ nodule measured with 1.2-mm³ precision, the 95% CI would be –12%, 52%. Therefore, knowledge of the precision for

TABLE 5
PVMs as a Group Compared with Threshold Methods and VTMs

Factor	P Values*	
	PVMs vs Threshold Methods	PVMs vs VTMs
Size (mm ³)		
Small (8–18)	.009	.040
Large (35–61)	.038	.041
Tube current time (mAs)		
20	.038	.006
120	.158	.486
Attenuation		
Ground glass	.026	.038
Solid	.020	.033

Note.—Threshold methods include FTM, VTM1, and VTM2. VTMs include VTM1 and VTM2.
* One-tailed test, with $P < .05$ considered to indicate a significant difference.

volume measurements is essential for correct interpretation of nodule growth.

Results in the current study demonstrate good correlation between two independent observers. Despite the need for manual sampling, all methods yielded acceptable and high inter- and intraexaminer reliability. In the near future, the manual sampling of nodule attenuation and lung background can be readily automated, although implementation of placement of the large ROI and full automation may be difficult secondary to the presence of vessels in the human lung.

In the current study, we demonstrated an increase of at least 0.48 mm³ and a mean increase of 0.86 mm³ in precision of volume measurement when the technique was changed from 20 mAs (tube current of 40 mA with our parameters), which is used to perform low-dose chest CT, to 120 mAs, which is used to perform diagnostic CT. Low-dose chest CT is typically performed with tube currents between 20 and 50 mA (5,29–31). Given the small difference in precision and the benefit of lower radiation exposure to patients, the use of low-dose technique for the follow-up of nodules detected at screening CT is a consideration and a topic for future study.

In our study, a high-frequency reconstruction algorithm provided more precise quantification of pulmonary nodules, and we propose reconstruction of image data by means of a high-frequency algorithm when volume quantification is planned. Greater precision may be related to the higher spatial resolution that a high-frequency algorithm provides (32), which facilitates the sampling of small 2–3-mm nodules. Nodule location and distance to pleura did not significantly affect volume measurement. Results of prior work on nodule densitometry in phantoms demonstrate that

TABLE 6
Error in Nodule Volume Measurements: Effect of Nodule Volume

Method	Approximate Nodule Volume (mm ³)	
	Approximately 8–18	Approximately 35–61
PVM		
PVMA	1.2 ± 0.9	2.1 ± 1.5
PVM1	1.2 ± 1.0	2.6 ± 1.6
PVM2	2.0 ± 1.9	2.5 ± 1.4
Threshold		
VTM1	1.9 ± 1.6	2.8 ± 1.7
VTM2	2.4 ± 3.4	3.0 ± 2.9
FTM	4.0 ± 2.2	10.1 ± 3.6

Note.—Data are mean absolute error (mm³) ± SD.

beam-hardening artifact associated with chest-wall structures lowered attenuation by approximately 20 HU (20). These differences were likely too small to influence the quantitative methods used in our study. Additionally, in prior studies, inhomogeneity associated with object position in the field of view created attenuation differences of 50 HU (20). Such differences may have been minimized in our study if the CT scanner had equally responsive detectors and a homogeneous radiation beam. Sampling of pure nodule and pure lung measurements from the same vicinity may have overcome both artifact and inhomogeneities related to position.

We emphasize that the present study was performed in a phantom model, which likely results in underestimation of the errors that occur when quantitative methods are applied in vivo. The presence of normal structures, such as vessels and bronchi, or heterogeneity in the surrounding lung, as may result from

emphysema, pneumonia, or infiltrative lung disease, may negatively affect volume quantification. In this study, we attempted to simulate variation in the lung parenchyma attenuation by surrounding the nodules with a heterogeneous material. The influence of intervening discrete structures and other factors on volume measurement and detection of growth will need to be clarified in future studies. Use of a PVM, which does not rely on precise binary segmentation of a nodule, may overcome these obstacles.

We did not address the measurement of spiculated and grossly nonspherical nodules or subsolid nodules with mixed ground-glass and solid attenuation. Additionally, we did not use images reconstructed on the basis of transverse intervals of less than 1.0 mm. While this may be clinically feasible in the future, our goal was to investigate imaging protocols that were being used with the available multi-detector row CT technology, which provides high-resolution 1.0-mm-thick sections for nodule analysis that were obtained during the same breath hold. Rather than use a smaller field of view that increased spatial resolution, we chose to use a field of view that encompassed the entire thorax so that we could evaluate the volume errors of nodules on high-resolution data without needing to selectively target reconstructions to specific nodules. Use of a smaller field of view would likely lead to more accurate volume estimates. On the other hand, respiratory motion would likely decrease the precision for all methods, given the creation of artifacts, and in the future could be minimized by using CT scanners with faster rotation speeds.

In summary, a PVM approach is a promising method for quantification of nodule volume and follow-up of nodules discovered at low-dose and diagnostic CT. Results in our study suggest that use of a PVM and a high-frequency reconstruction algorithm will yield improved precision in volume quantification.

Acknowledgments: The authors acknowledge Cornel Stefanescu for his expert technical assistance with phantom construction. Emilio Vega, RT, Fiona Feeley, RT, and Bernard Assadurian, RT, are thanked for their technical assistance with CT. All are from the Department of Radiology at New York University Medical Center.

References

- Zerhouni EA, Stitik FP, Siegelman SS, et al. CT of the pulmonary nodule: a cooperative study. *Radiology* 1986; 160:319-327.
- Klein JS, Salomon G, Stewart EA. Trans-thoracic needle biopsy with a coaxially placed 20-gauge automated cutting needle: results in 122 patients. *Radiology* 1996; 198:715-720.
- Swensen SJ. Functional CT: lung nodule evaluation. *RadioGraphics* 2000; 20:1178-1181.
- Patz EF, Lowe VJ, Hoffman JM, et al. Focal pulmonary abnormalities: evaluation with F-18 fluorodeoxyglucose PET scanning. *Radiology* 1993; 188:487-490.
- Henschke CI, McCauley DI, Yankelevitz DF, et al. Early Lung Cancer Action Project: overall design and findings from baseline screening. *Lancet* 1999; 354:99-105.
- Munden RF, Pugatch RD, Liptay MJ, Sugarbaker DJ, Le LU. Small pulmonary lesions detected at CT: clinical importance. *Radiology* 1997; 202:105-110.
- Siegelman SS, Khouri NF, Leo FP, Fishman EK, Braverman RM, Zerhouni EA. Solitary pulmonary nodules: CT assessment. *Radiology* 1986; 160:307-312.
- Zwirer CV, Vedal S, Miller RR, Muller NL. Solitary pulmonary nodule: high-resolution CT and radiologic-pathologic correlation. *Radiology* 1991; 179:469-476.
- Nathan MH, Collins VP, Adams RA. Growth rates in benign and malignant pulmonary nodules. *Radiology* 1962; 79:221-231.
- Weiss W. Peripheral measurable bronchogenic carcinoma: growth rate and period of risk after therapy. *Am Rev Respir Dis* 1971; 103:198-208.
- Aoki T, Nakata H, Watanabe H, et al. Evolution of peripheral lung adenocarcinomas: CT findings correlated with histology and tumor doubling time. *AJR Am J Roentgenol* 2000; 174:763-768.
- Schwartz LH, Ginsberg MS, DeCorato D, et al. Evaluation of tumor measurements in oncology: use of film-based and electronic techniques. *J Clin Oncol* 2000; 18:2179-2184.
- Harris KM, Adams H, Lloyd DC, Harvey DJ. The effect on apparent size of simulated pulmonary nodules of using three standard CT window settings. *Clin Radiol* 1993; 47:241-244.
- Wormanns D, Diederich S, Lentschig MG, Winter F, Heindel W. Spiral CT of pulmonary nodules: interobserver variation in assessment of lesion size. *Eur Radiol* 2000; 10:710-713.
- Yankelevitz DF, Gupta R, Zhao B, Henschke CI. Small pulmonary nodules: evaluation with repeat CT—preliminary experience. *Radiology* 1999; 212:561-566.
- Yankelevitz DF, Reeves AP, Kostis WJ, Zhao B, Henschke CI. Small pulmonary nodules: volumetrically determined growth rates based on CT evaluation. *Radiology* 2000; 217:251-256.
- Reeves AP, Kostis WJ, Yankelevitz DF, Henschke CI. Analysis of small pulmonary nodules without explicit segmentation of CT images (abstr). *Radiology* 2000; 217(P):243.
- Naidich DP, Marshall CH, Gribbin C, Arams RS, McCauley DI. Low-dose CT of the lungs: preliminary observations. *Radiology* 1990; 175:729-731.
- Itoh S, Ikeda M, Arahata S, et al. Lung cancer screening: minimum tube current required for helical CT. *Radiology* 2000; 215:175-183.
- Zerhouni EA, Spivey JF, Morgan RH, Leo FP, Stitik FP, Siegelman SS. Factors influencing quantitative CT measurements of solitary pulmonary nodules. *J Comput Assist Tomogr* 1982; 6:1075-1087.
- McCullough EC, Morin RL. CT-number variability in thoracic geometry. *AJR Am J Roentgenol* 1983; 141:135-140.
- Zerhouni EA, Boukadoum M, Siddiky MA, et al. A standard phantom for quantitative CT analysis of pulmonary nodules. *Radiology* 1983; 149:767-773.
- Rusinek H, Naidich DP, McGuinness G, et al. Pulmonary nodule detection: low-dose versus conventional CT. *Radiology* 1998; 209:243-249.
- Fleiss JL. The design and analysis of clinical experiments. New York, NY: Wiley, 1986.
- Boiselle PM, Ernst A, Karp DD. Lung cancer detection in the 21st century: potential contributions and challenges of emerging technologies. *AJR Am J Roentgenol* 2000; 175:1215-1221.
- Therasse P, Arbuck SG, Eisenhauer EA, et al. New guidelines to evaluate the response to treatment in solid tumors. European Organization for Research and Treatment of Cancer, National Cancer Institute of the United States, National Cancer Institute of Canada. *J Natl Cancer Inst* 2000; 92:205-216.
- Joe BN, Fukui MB, Meltzer CC, et al. Brain tumor volume measurement: comparison of manual and semiautomated methods. *Radiology* 1999; 212:811-816.
- Yankelevitz DF, Henschke CI. Derivation for relating calcification and size in small pulmonary nodules. *Clin Imaging* 1998; 22:1-6.
- Swensen SJ, Jett JR, Sloan JA, et al. Screening for lung cancer with low-dose spiral computed tomography. *Am J Respir Crit Care Med* 2002; 165:508-513.
- Diederich S, Wormanns D, Semik M, et al. Screening for early lung cancer with low-dose spiral CT: prevalence in 817 asymptomatic smokers. *Radiology* 2002; 222:773-781.
- Sone S, Li F, Yang ZG, et al. Results of three-year mass screening programme for lung cancer using mobile low-dose spiral computed tomography scanner. *Br J Cancer* 2001; 84:25-32.
- Bushberg JT, Seibert JA, Leidholdt EM Jr, Boone JM. The essential physics of medical imaging. Baltimore, Md: Williams & Wilkins; 1994.